Nano-sized SnO$_2$ Photocatalysts: Synthesis, Characterization and Their Application for the Degradation of Methylene Blue Dye

M. T. Uddin[*], Y. Sultana, M. A. Islam

Department of Chemical Engineering and Polymer Science, Shahjalal University of Science and Technology Sylhet-3114, Bangladesh

Abstract

In the present study, tin oxide (SnO$_2$) nanoparticles were prepared by precipitation method using tin tetrachloride (SnCl$_4$) as precursor and ammonia solution as precipitating agent followed by calcination at 400 ºC for 2 h. As-prepared SnO$_2$ particles were characterized by X-ray diffraction (XRD) and Fourier Transform Infrared (FTIR). The powder XRD results revealed that the SnO$_2$ nanoparticles had a typical tetragonal rutile (cassiterite) structure and the average crystallite size calculated by using the Debye –Scherrer equation was found to be approximately 5.1 nm. The photocatalytic activity of the as-prepared photocatalysts was investigated by degrading methylene blue (MB) dye. The effect of pH, catalyst loading and initial dye concentration on photocatalytic degradation was investigated. Results showed that the SnO$_2$ nanoparticles represented excellent photocatalytic activity for the degradation of MB under UV light with 200 min of irradiation time. The results also showed that the pH of solution had a direct influence on the photocatalysis process and basic pH was favorable for the degradation of MB. The effect of pH on photocatalytic activity was explained with the help of zero point charge (pH$_{pzc}$). Furthermore, the photocatalysts could be easily recycled without significant change in the catalytic activity.

Keywords: Nanoparticles; SnO$_2$; Photocatalyst; Photodegradation; Methylene blue.

1. Introduction

Rapid industrial growth and the worldwide population explosion have resulted in a large escalation of demand for fresh water, both for the household needs and for crops to produce adequate quantities of food. Besides other needs the demand for water has increased tremendously with agricultural, industrial and domestic sectors consuming 70, 22 and 8% of the available fresh water, respectively and this has resulted in the generation of large amounts of wastewater containing a number of pollutants [1,2]. One of the

---

[*] *Corresponding author:* mtuddin-cep@sust.edu

important classes of the pollutants is dyes. It is estimated that over 10,000 different dyes and pigments are used industrially and over 7×10^5 tons of synthetic dyes are annually produced worldwide [3]. In the textile industry, up to 200,000 tons of these dyes are lost to effluents every year during dyeing and finishing operations as a result of inefficiency in the dyeing process [3,4]. Dyes are widely used in various industries-for example, paints, textiles, leather, papers, and so on. However, most industrial dyes are toxic, carcinogenic, and mutagenic, and have low biodegradability. Moreover, dye-containing effluents are highly colored, so discarding these effluents into natural water bodies affects the balance of aquatic ecosystems because they can prevent the penetration of sunlight into the water, which results in a reduction in dissolved oxygen content [5]. Therefore, the removal of dyes prior to the discharge of wastewater from dye industries is of great importance.

The possible methods of dye removal from industrial effluents include adsorption, chemical coagulation, flocculation, precipitation, chemical oxidation, froth floatation, ozonation, reverse osmosis and biological techniques [6]. Although the above mentioned physical and/or chemical methods have been widely used, they possess inherent limitations such as high cost, formation of hazardous byproducts and intensive energy requirements. The conventional methods, such as coagulation and flocculation, used for the removal of dyes from water introduce metallic impurities and produce a large amount of sludge which requires further disposal. Biological treatment requires a large land area and is constrained by sensitivity toward diurnal variation as well as toxicity of some chemicals, and less flexibility in design and operation [7]. Although many organic molecules are degraded, many others are recalcitrant due to their complex chemical structure and synthetic organic origin [8]. On the other hand, chemical techniques use huge amount of chemical and produce large volume of sludge which itself requires treatment. This method is also very expensive. The major disadvantage of the membrane processes (nanofiltration, reverse osmosis, electrodialysis, . . .) is that they have a limited lifetime before membrane fouling occurs and the cost of periodic replacement must thus be included in any analysis of their economic viability. Therefore, it is a challenge today to develop sustainable and economically viable technology to treat, recycle and reuse of dye containing wastewater. In these cases, it is necessary to adopt reactive systems much more effective than those adopted in conventional purification processes. Therefore, the development of eco-friendly methods of destroying these pollutants became an imperative task.

Over the past decade, many research efforts have been devoted around the world to develop a newer, more powerful, and very promising technique called Advanced Oxidation Processes (AOPs) to treat the contaminants of drinking water and industrial effluents. Conventional AOPs can be classified as homogeneous and heterogeneous processes, depending on whether they occur in a single phase or they make use of a heterogeneous catalyst like metal supported catalysts, carbon materials or semiconductors such as TiO_2, ZnO, and WO_3. One of the AOPs is a semiconductor-based photocatalysis process which involves the complete photo-mineralization or oxidation by generation of hydroxyl radicals that reacts with most of the organics and mineralizes them into CO_2,

H_2O and inorganic ions including PO_4^{3-}, NO^{3-}, and halide ions without further production of intermediate toxic byproducts [9,10]. Photocatalytic degradation generally involves the complete photomineralization or oxidation of the target contaminants into H_2O, CO_2.

Metal oxide nanoparticles have gained increasing importance as the nano-sized particles increase the exposed surface area of active catalyst components which results in dramatically enhancing the contact between reactants and the catalyst. Tin oxide (SnO_2) is one of the most intensely studied n-type semiconductor. During the past decade, SnO_2 has been widely used in solid-state gas sensors [11], transparent conducting electrodes [12], rechargeable Li batteries [13], optical electronic devices [14] and solar cells [15]. The structure, bandgap, and chemical stability of SnO_2 are similar to those of titanium dioxide, which is widely used photocatalyst. Moreover, SnO_2 has no adverse health effects and is poorly absorbed by the human body when injected or inhaled [16]. Thus, SnO_2 is potentially an ideal photocatalyst.

Although there has been considerable success in the synthesis of SnO_2 nanomaterials of various morphologies [17-20], it is still a major challenge to prepare SnO_2 nanocrystals (NCs) with dimensions of less than 10 nm in different discrete sizes and relatively high BET surface area which is essential features for higher photocatalytic activity [21,22]. Furthermore, to date, many SnO_2-based coupled semiconductor composite photocatalysts, such as SnO_2-TiO_2 [23-26], SnO_2-ZnO [27-31] or SnO_2-CuO [32] have been extensively studied for their high photocatalytic activities. But the study about SnO_2 [33-37] is especially less. In addition, the problem of simultaneous formation of Sn^{2+} and even Sn^0, leads to the mixed phases of SnO_2 and SnO or Sn present in the catalyst [38,39]. It is thus highly desirable to develop a facile and reproducible method to synthesize well-defined phase-pure SnO_2.

In this study, SnO_2 nanoparticles with small crystallite size have been synthesized by a precipitation method. The resulting photocatalysts were characterized by Fourier transform infrared (FTIR) spectroscopy and X-ray diffraction (XRD). The pH at the point of zero charge, pH_{PZC}, of the synthesized photocatalysts was determined by titration method. The photocatalytic activity of the photocatalysts was investigated by the degradation of methylene blue (MB) dye under UV irradiation. Here, MB has been used as a model dye. The photocatalytic activity of recycled SnO_2 composite was also investigated.

2. Experimental

2.1. *Chemicals*

Anhydrous $SnCl_4$ (Sigma Aldrich), 25% ammonia solution (Merck) methylene blue (Loba Chemie) were of analytical grade and used as received without further purification. Distilled water was used to prepare the desired solutions in all experiments. The pH of the solution was adjusted to the desired value by dilute HCl and NaOH solutions.

2.2. *Preparation of SnO$_2$ photocatalysts*

All the chemicals were analytical grade and used without further purification. Nanocrystalline SnO$_2$ was prepared by homogeneous precipitation method. Anhydrous SnCl$_4$ was used as the starting material and ammonia solution was used as the precipitant. In a typical preparation procedure, 5 mL SnCl$_4$ was dissolved into 20 mL distilled water to form a transparent solution. Ammonia solution was then added drop-wise into the SnCl$_4$ solution under magnetic stirring. The precipitate of SnO$_2$ was appeared with the addition of ammonia solution. When the precipitation was complete, the resulting solution was continually stirred for another 18 h. Subsequently, precipitate was separated by centrifugation at 5800 rpm followed by successive washing with distilled water until no traces of chloride ion was found in the filtrate.

The resulting wet powder was then dried in a muffle furnace at about 125°C for 8 h. followed by calcinations at 400°C for 2 h. The calcined powder was then ground and used for photocatalytic experiment.

2.3. *Characterization of photocatalyst*

To determine the phase structures and crystallite size of the heterostructure SnO$_2$ photocatalyst powder, XRD measurement was carried out by X-ray diffractometer (Bruker AXS, D8 Advance) using CuK_α radiation. A continuous scan mode was used to collect 2θ data from 10 to 90°. The average crystallite size of the powder was determined from the diffraction peak widths using Scherrer's formula.

FTIR analysis was applied to determine the surface functional groups, using FTIR spectroscope (Japan Shimadzu IR). Samples were diluted with KBr and pressed into a disk shape prior to FTIR analysis. FTIR spectra were recorded in the range of 450-4000 cm^{-1}.

By definition, pH$_{PZC}$ is the pH of the solution in contact with solid at which the net surface charge on the surface of a particle is zero. The pH$_{PZC}$ of the SnO$_2$ was measured by the pH drift method. The determination of pH$_{PZC}$ was done by adjusting the pH of 0.01 M NaCl (50 mL) to values between 2 and 10 obtained by adding either 0.1 M HCl or NaOH solution. About 0.1 g of SnO$_2$ was added into each solution at room temperature and then shaken for 48 h. The final pH was measured and plotted against the initial pH. The pH at which the plotted curve intersects the line of pH (final) = pH (initial) was taken as the pHpzc of the SnO$_2$ surface.

2.4. *Photocatalytic experiment*

Photocatalytic activities of synthesized samples were evaluated by the degradation of MB dye. In each experiment, 0.25 g photocatalyst was dispersed in 800 mL of MB solution (10 mg/L). The experiments were carried out in a pyrex beaker illuminated with a 6 W high pressure mercury lamp (Model: SB-6/T5, IN: 200-240V, 50/60 Hz, .03A, Power;

6W, Cosø: 0.6) under continuous stirring. The UV lamp was positioned vertically into the solution. Prior to irradiation, the suspension was stirred in dark for 30 min. to reach adsorption/desorption equilibrium. Samples were taken from the reaction suspension at a predetermined time interval. The upper clear liquid obtained after centrifugal separation was analyzed by UV–vis spectroscopy (UV-1650, Shimadju, Japan) at the maximum absorption wavelength of MB of 664 nm. A blank experiment without UV irradiation but with SnO_2 photocatalysts was performed. Another blank experiment without SnO_2 photocatalysts but with UV irradiation was also performed. The degradation efficiency (*D*) was defined by the following equation:

$\%D = (C_0\text{-}C)/C_0 \times 100\%$

where C_0 is the initial concentration and *C* is the concentration of dye at the reaction time.

3. Results and Discussion

3.1. Characterization

The FTIR spectroscopy is usually used to determine the functional groups. The FTIR spectra of the synthesized SnO_2 nanoparticles are shown in Fig.1: (a) before calcination and (b) after calcination. Fig. 1(a), the spectrum before calcination, shows that the peaks in the FTIR pattern at about 3300–3420 cm^{-1} and 1620 cm^{-1} can be attributed to the stretching vibration of O–H groups and the bending vibration of adsorbed molecular water, respectively [40-42]. The peak at around 1410 cm^{-1} was assigned to NH deformation of ammonia [42]. The bands at around 640 cm^{-1} and 520 cm^{-1} were attributed to Sn-O stretching modes of Sn-O-Sn and Sn-OH, respectively [43,44]. These bands show that before calcination, not all $Sn(OH)_4$ had undergone a condensation reaction to form SnO_2.

Fig. 1 (b) shows that the peak appeared from ammonia before calcination almost disappeared when the product was calcined at 400 °C for 2 h. The intensity of the band at 3300-3420 was reduced after cancination. This shows the removal of hydroxyl groups during calcinations. The peak at about 640 and 520 cm^{-1} became stronger and weaker, respectively, because a condensation reaction occurred between Sn-OH groups during calcinations to form Sn-O-Sn.

The crystalline phase composition and the size of crystallite of synthesized SnO_2 photocatalyst were determined by XRD. The X-ray diffraction pattern of tin oxide powder prepared by precipitation method is shown in Fig. 2. All the diffraction peaks are quite similar to those of SnO_2, which can be indexed as the tetragonal rutile (cassiterite) structure of SnO_2 with lattice constants of a = 4.73650 Å and c = 3.20100 Å, which is in good agreement with the JCPDS file of SnO_2 (JCPDS card no. 41 - 1445). No impurity diffraction peaks are observed, indicating the high purity of the final products. However, the intensities of diffraction peaks are relatively weak and broad compared to those of bulk SnO_2, which is attributed to the low crystallinity and small crystallite size of the SnO_2 particles. Furthermore, the average crystallite size (*d*) of the prepared SnO_2 can be

calculated from the strongest (110) plane diffraction peak ($2\theta = 26.64$) by applying the Debye–Scherrer equation:

$$d = k\lambda / \beta \cos\theta \qquad\qquad (1)$$

where d is the average crystallite size, λ is the X-ray wavelength, β is the full width at half maximum (FWHM) of the diffraction peak, θ is the Bragg diffraction angle and k is the so-called shape factor whose value is about 0.9. According to this equation, the average crystallite size of the prepared SnO_2 was approximately 5.1 nm.
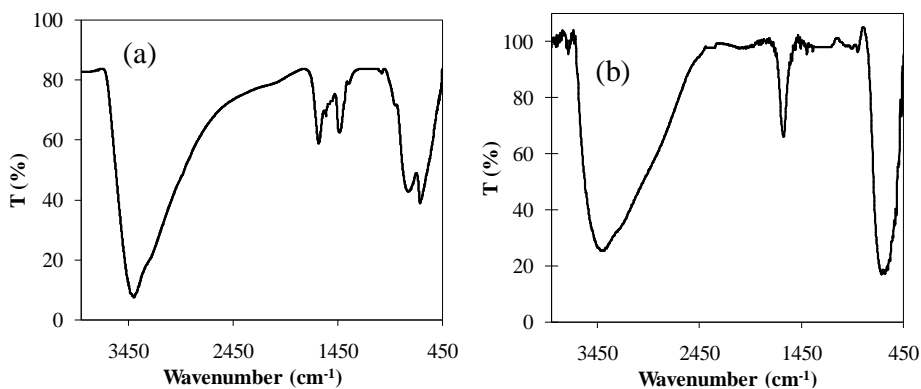
Fig. 1. FTIR spectra of SnO_2 nanoparticles (a) before calcination and (b) after calcination.
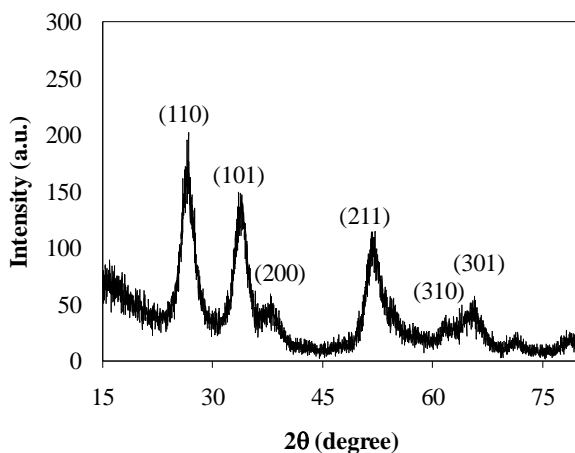

Fig. 2. XRD pattern of calcined SnO_2 nanoparticles.

The pH at the point of zero charge is important because it indicates the net surface charge of the photocatalysts which in turn affect the photocatalytic activity. To determine the pH_{PZC}, the pH drift method was used. The experimental results are shown in Fig. 3. The pH_{PZC} is the point where the curve of pH_{final} vs $pH_{initial}$ intersects the line $pH_{initial} = pH_{final}$, with the value for the synthesized SnO_2 nanoparticles being 5.0.

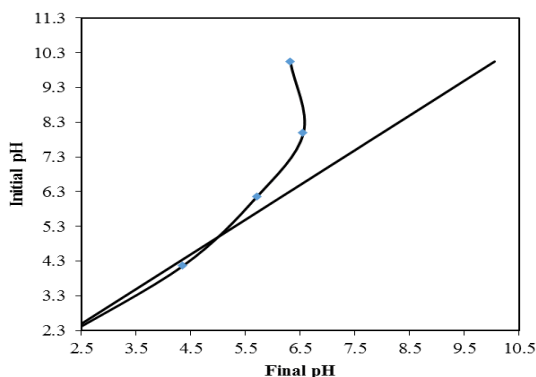Fig. 3. Point of zero charge (pH$_{PZC}$) of the activated carbon determined by the pH drift method.

3.2. *Photocatalytic study*

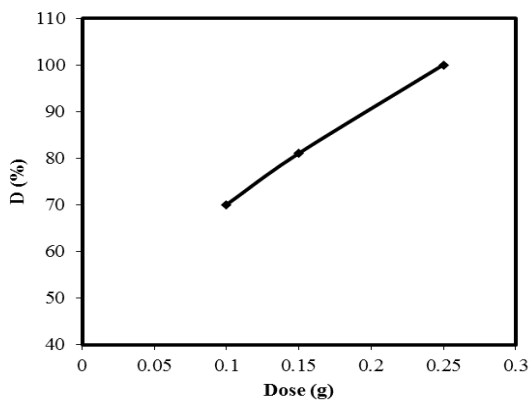### 3.2.1. *Effect of doses on the photocatalytic activity of SnO$_2$*

Fig. 4. Effect of dosage on the photocatalytic activity. Conditions: volume, $V = 800$ mL, initial dye concentration = 10 mg/L, pH = 7.

The photocatalytic degradation of MB over different quantity of SnO$_2$ was investigated and the result is shown in Fig. 4. As shown in Fig. 4, the photocatalytic activity increased with increasing catalyst loading. The degradation efficiency increased from 70% to 100% when the catalyst loading increased from 0.10 g to 0.25 g. This phenomenon could be explained as following: when the catalyst loading was small, the photon absorbed by catalyst and utilized for the photocatalytic reaction was also few, which resulted in low photocatalytic activity. With the increase of the catalyst loading, the number of photon absorbed and active centers on the surface of catalyst increased, resulting in the improvement of the activity.

3.2.2. *Effect of initial concentration on the photocatalytic activity*

It is well known that the initial concentration of reactant plays an important role on the photo-degradation of organic compounds. The influence of initial dye concentration on degradation was examined in the range of 5–25 mg/L with 0.25 g/800 mL catalyst loading. The percentage degradation as a function of initial dye concentration is shown Fig. 5. The result shows that the photo-degradation of the dye decreased at higher concentrations. With increasing the amounts of dyes, the more of dye molecules was adsorbed on the surface of the photocatalyst and the active sites of the catalysts was reduced resulting in the lower generation of hydroxyl radicals. Also, increasing concentration of dye decreased the number of photons that was arrived to the surface of catalysts. The more light was absorbed by molecules of dye and the excitation of photocatalyst particles by photons was reduced. Thus, photo-degradation efficiency was diminished.
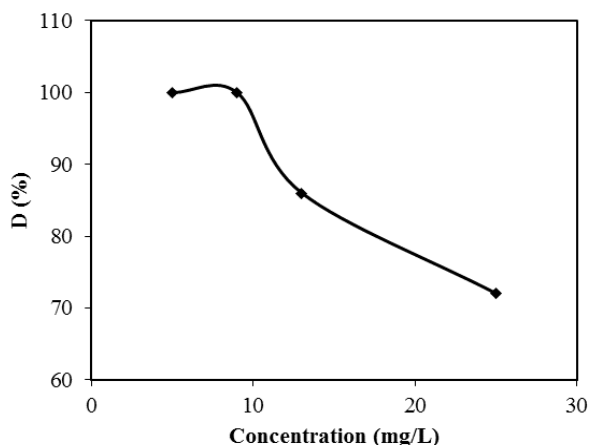

Fig. 5. Effect of initial MB dye concentration on the photocatalytic activity. Conditions: $V = 800$ mL, dose $= 0.25$ g, pH $= 7$.

3.2.3. *Effect of pH on the photocatalytic activity*

In photocatalysis systems, pH can be considered as one of the most important parameters that can greatly affect the photo-oxidation process. The effect of pH on the efficiency of photocatalytic degradation of MB was examined at the pH = 3, 7.4 and 10. The photocatalytic degradation efficiency of MB solution as a function of pH is shown in Fig. 6. The results showed that the pH of solution had a direct influence on the heterogeneous photocatalysis process. As observed in Fig. 6, the efficiency was more in alkaline solutions than that in acidic solutions. This is indicative of the significant role of the surface properties of the SnO₂ photocatalyst; the acid-base property of the metal oxide surface has a considerable influence on the photocatalytic efficiency with varying pH.
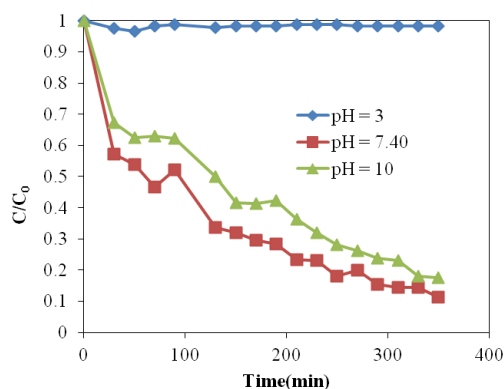
Fig. 6. Effect of pH on the photocatalytic activity of SnO_2. Conditions: V = 800 mL, dose = 0.25 g, concentration = 10 mg/L.

Considering the positive charge of cationic MB dye in solution, the effect of pH on the photocatalytic degradation of MB can be rationalized on the basis of electrostatic adsorption model where cations are more readily accumulated at the negative sites on SnO_2. This can be explained on the basis of pH_{zpc} of SnO_2 particle. The pH_{pzc} of SnO_2 powder was about pH 5. Above this pH value, the surfaces of SnO_2 particles were negatively charged, while below this pH value, they are positively charged. Since MB is a cationic dye, high pH favors adsorption on the catalyst surface which results in high degradation efficiency. On the other hand, at lower pH the electrostatic repulsion between the MB cations and positively charged oxide surface greatly reduces the adsorption of the MB dye resulting drastic decrease in degradation rate. Moreover, the pH of the solution affected the formation of hydroxyl radicals by the reaction between hydroxide ions and photo-induced holes on the SnO_2 surface. The positive holes are considered as the major oxidation steps at low pH, whereas hydroxyl radicals are considered as the predominant species at neutral or high pH levels [27]. It would be expected that the generation of •OH were higher due to the presence of more available hydroxyl ions on the SnO_2 surface. Thus the degradation efficiency of the process was logically enhanced at high pH.

3.2.4. Recyclability

For the purpose of practical implementation, it is essential to evaluate the stability and reuse of the catalyst. Fig. 7 shows the repetitive photo-degradation of MB during two consecutive cycles with the same 0.25 g/800 mL catalyst at 6 mg/L dye concentration. After each cycle, the SnO_2 catalyst was recovered and a fresh solution of MB was added before each photocatalytic run. The photocatalytic efficiency for the two cycling reuse were 100% and 94% after 170 min. of reaction time, respectively. No significant change in the catalytic efficiency of the degradation of MB dye by the photocatalysts after successive cycles of use under UV irradiation indicated the stability and reproducibility of

the catalysts. Slight decrease in the degradation efficiency in the second run was due to loss of catalyst during recovery.
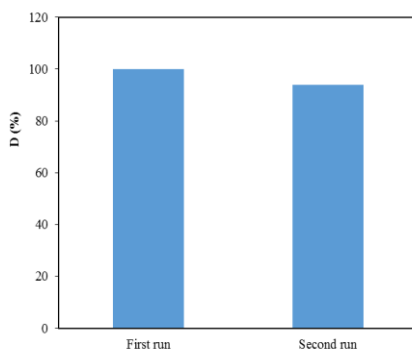

Fig. 7. Cyclic runs in the photo-degradation of MB employing SnO_2 under UV light. Conditions: V = 800 mL, dose = 0.25 g, concentration = 10 mg/L, pH = 7.

3.2.5. *Photocatalytic degradation mechanism*

The adsorption mechanism is explained in Fig. 8. Under UV light irradiation, the electron in the VB of SnO_2 is excited to the CB by leaving a hole in the VB. These electron-hole pairs migrate to the surface of the catalyst and take part in redox reaction with the species present on the surface of the catalyst [37]. The photo-generated take part in the reduction of dissolved oxygen forming superoxide radical anions, $O_2^{\bullet-}$, yielding hydroperoxy radicals $HO_2^{\bullet}$ on protonation and finally $OH^{\bullet}$ radicals, while the photo-generated holes oxidize the surface hydroxyl group or physisorbed water molecules forming hydroxyl radical, $OH^{\bullet}$. $OH^{\bullet}$ radicals are a strong oxidizing agent well-known to decompose organic substrates as MB dye [15,37,46].

$$SnO_2 + h\nu \longrightarrow SnO_2.e_{cb}^- + SnO_2.h_{vb}^+$$

$$SnO_2.e_{cb}^- + O_2 \longrightarrow SnO_2 + O_2^{\bullet-}$$

$$SnO_2.h_{vb}^+ + OH^- \longrightarrow OH^{\bullet}$$

$$O_2^{\bullet-} + H_2O \longrightarrow HO_2^{\bullet} + OH^-$$

$$HO_2^{\bullet} + H_2O \longrightarrow HO^{\bullet} + H_2O_2$$

$$H_2O_2 \longrightarrow 2 OH^{\bullet}$$

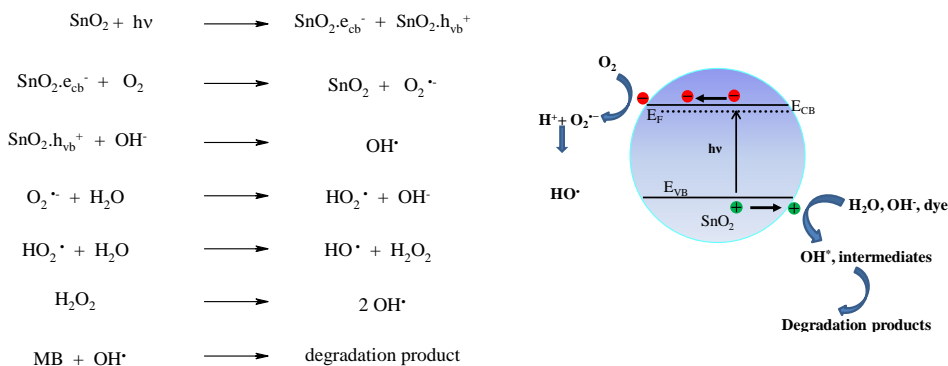$$MB + OH^{\bullet} \longrightarrow \text{degradation product}$$

Fig. 8. Schematic mechanism for the photocatalytic degradation of MB by SnO_2 nanoparticles.

4. Conclusion

Nanostructured SnO_2 photocatalysts have been successfully prepared by the homogenous precipitation method followed by calcination. The nanoparticles were a typical tetragonal rutile (cassiterite) structure and the average crystallite size was found to be approximately 5.1 nm. The synthesized SnO_2 nanoparticles represented excellent photocatalytic activity for the degradation of MB under UV light irradiation. The pH of solution had a direct influence on the photocatalysis process and basic pH was favorable for the degradation of MB. Furthermore, the photocatalysts could be easily recycled without significant change in the catalytic activity, which indicated the stability and reproducibility of the catalysts. This concept of semiconducting nanocatalysts with high photocatlytic activity should find industrial application in the future to remove undesirable organics from the environment.

References

1. I. Shiklamov, "World Water Resources. A New Appraisal and Assessment for the 21st Century." A Summary of the Monograph World Water Resources Prepared in the Framework of the International Hydrological Programme (UNESCO, Paris, 1998). http://biosinfonet.yolasite.com/resources/World%20water%20resources.pdf
2. 4th UN World Water Development Report, 2012.
3. H. Zollinger, Synthesis, Properties of Organic Dyes and Pigments. In: Color Chemistry (VCH Publishers, New York, USA, 1987) pp. 92-102.
4. C. J. Ogugbue and T.Sawidis, Biotechnol. Res. Int. 2011. http://dx.doi.org/10.4061/2011/967925
5. K. C. Chen, J. Y. Wu, D. J. Liou, and S. C. J. Hwang, J. Biotechnol. **101**, 57 (2003). http://dx.doi.org/10.1016/S0168-1656(02)00303-6
6. K. Rasool, S. H. Woo, and D. S. Lee, Chem. Eng. J. **223**, 611 (2013). http://dx.doi.org/10.1016/j.cej.2013.03.031
7. K. G. Bhattacharyya and A. Sharma, Dyes Pigm. **57**, 211 (2003). http://dx.doi.org/10.1016/S0143-7208(03)00009-3
8. M. N. V. R. Kumar, T. R. Sridhari, K. D. Bhavani, and P. K. Dutta, Colorage **45**, 25 (1998).
9. O. Carp, C. L. Huisman, and A. Reller, Prog. Solid State Chem. **32**, 33 (2004). http://dx.doi.org/10.1016/j.progsolidstchem.2004.08.001
10. S. P. Patil, V. S. Shrivastava, G. H. Sonawane, and S. H. Sonawane, J. Environ. Chem. Eng. **3**, 2597 (2015). http://dx.doi.org/10.1016/j.jece.2015.09.005
11. M. H. S. Abadi, M. N. Hamidon, A. H. Shaari, N. Abdullah, and R. Wagiran, Sensors **11**, 7724 (2011). http://dx.doi.org/10.3390/s110807724
12. K. L. Chopra, S. Major, and D. K. Pandya, Thin Solid Films **102**, 1 (1983). http://dx.doi.org/10.1016/0040-6090(83)90256-0
13. Z. Peng, Z. Shi, and M. Liu, Chem. Commun. **2000**, 2125. http://dx.doi.org/10.1039/b007687m
14. A. Aoki and H. Sasakura, Jpn. J. Appl. Phys. **9**, 582 (1970). http://dx.doi.org/10.1143/JJAP.9.582

15. Z. Tebby, M. T. Uddin, Y. Nicolas, C. Olivier, T. Toupance, C. Labrugère, and L. Hirsch, ACS Appl. Mater. Interface **3**, 1485 (2011). http://dx.doi.org/10.1021/ic300794j
16. X. Zhu, Z. Guo, P. Zhang, Guo, G. Du, R. Zeng, H. Liu, and Z. Chen, ChemPhysChem **10,** 3101 (2009). http://dx.doi.org/10.1002/cphc.200900546
17. S. Wu, Q. Cao, S. Yin, X. Liu, and X. Zhang, J. Phys. Chem. C **113**, 17893 (2009). http://dx.doi.org/10.1021/jp901221h
18. H. J. Wang, F. Q. Sun, Y. Zhang, L. S. Li, H. Y. Chen, Q. S. Wu, and J. C. Yu, J. Mater. Chem*. **20**, 5641 (2010). http://dx.doi.org/10.1039/b926930d
19. X. X. Xu, J. Zhuang, and X. Wang, J. Am. Chem. Soc. **130**, 12527 (2008). http://dx.doi.org/10.1021/ja077102a
20. G. S. Peng, S. G. Chen, Y. Koltypin, A. Zaban, S. H. Feng, and A. Gedanken, Nano Lett. **1**, 723 (2001). http://dx.doi.org/10.1021/nl0156181
21. N. Sergent, P. Gelin, L. P. Camby, H. Praliaud, and G. Thomas, Sens. Actuators B **84**, 176 (2002). http://dx.doi.org/10.1016/S0925-4005(02)00022-9
22. M. Zhang, G. Sheng, J. Fu, T. An, X. Wang, and X. Hu, Mater. Lett. **59**, 3641 (2005). http://dx.doi.org/10.1016/j.matlet.2005.06.037
23. M. F. A. Messih, M. A. Ahmed, and A. S. E. Syhed, J. Photochem. Photobiol. A **260**, 1(2013)**.** http://dx.doi.org/10.1016/j.jphotochem.2013.03.011
24. L. R. Hou, C. Z. Yuan, and Y. J. Peng, Hazard. Mater. B **139**, 310 (2007)**.** http://dx.doi.org/10.1016/j.jhazmat.2006.06.035
25. L. Shi, C. Li, H. Gu, and D. Fang, Mater. Chem. Phys. **62**, 62 (2000). http://dx.doi.org/10.1016/S0254-0584(99)00171-6
26. J. Yang, D. Li, X. Wang, X. Yang, and L. Lu, J. Solid State Chem. **165**, 193 (2002). http://dx.doi.org/10.1006/jssc.2001.9526
27. M. T. Uddin, Y. Nicolas, C. Olivier, T. Toupance, L. Servant, M. M. Müller, H. J. Kleebe, J. Ziegler, and W. Jaegermann, Inorg. Chem. **51**, 7764 (2012). http://dx.doi.org/10.1021/ic300794j
28. C. C. Lin and Y. J. Chiang, Chem. Eng. J. **181-182**, 196 (2012). http://dx.doi.org/10.1016/j.cej.2011.11.062
29. Z. Yang, L. Lv, Y. Dai, Z. Xv, and D. Qian, Appl. Surf. Sci. **256**, 2898 (2010). http://dx.doi.org/10.1016/j.apsusc.2009.11.047
30. Z. Wen, G. Wang, W. Lu, Q. Wang, Q. Zhang, and J. Li, Cryst. Growth Des. **9**, 1722 (2007). http://dx.doi.org/10.1021/cg060801z
31. M. Davis, W. M. Hikal, C. Gümeci, and L. J. H. Weeks, Catal. Sci. Technol. **2**, 922 (2012). http://dx.doi.org/10.1039/c2cy20020a
32. H. L. Xia, H. S. Zhang, T. Zhuang, and D. C. Xiao, J. Environ. Sci. **19**, 1141 (2007). http://dx.doi.org/10.1016/S1001-0742(07)60186-7
33. Z. He and J. Zhou, Mod. Res. Catal. **2**, 13 (2013). http://dx.doi.org/10.4236/mrc.2013.23A003
34. M. Dimitrov, T. Tsoncheva, S. Shao, and R. Kohn, Appl. Catal. B **94**, 158 (2010). http://dx.doi.org/10.1016/j.apcatb.2009.11.004
35. Y. T. Han, X. Wu, Y. L. Ma, L. H. Gong, F. Y. Qu, and H. J. Fan, Cryst. Eng. Comm. **13**, 3506 (2011). http://dx.doi.org/10.1039/c1ce05171g
36. S. S. Wu, H. Q. Cao, S. F. Yin, X. W. Liu, and X. R. Zhang, J. Phys. Chem. C **113**, 17893 (2009). http://dx.doi.org/10.1021/jp9068762
37. S. P. Kim, M. Y. Choi, and H. C. Choi, Mater. Res. Bull. **74**, 85 (2016). http://dx.doi.org/10.1016/j.materresbull.2015.10.024
38. S. Tsunekawa, J. Kang, K. Asami, Y. Kawazoe, and A. Kasuya, Appl. Surf. Sci. **201**, 69 (2002). http://dx.doi.org/10.1016/S0169-4332(02)00516-0
39. R. Ramamoorthy, M. K. Kennedy, H. Nienhaus, A. Lorke, F.E. Kruis, and H. Fissan, Sens. Actuators B-Chem. **88**, 281 (2003). http://dx.doi.org/10.1016/S0925-4005(02)00370-2
40. L. Xi, D. Qian, X. Tang, and C. Chen, Mater. Chem. Phys. **108**, 232 (2008). http://dx.doi.org/10.1016/j.matchemphys.2007.09.023

41. S. Zhan, D. Li, S. Liang, X. Chen, and X. Li, Sensors **13**, 4378 (2013). http://dx.doi.org/10.3390/s130404378
42. T. Krishnakunar, N. Pinna, K. P. Kumari, K. Perumal, and R. Jayaprakash, Mater. Lett. **62**, 3437 (2008). http://dx.doi.org/10.1016/j.matlet.2008.02.062
43. K. C. Song and Y. Kang, Mater. Lett. **42**, 283 (2000). http://dx.doi.org/10.1016/S0167-577X(99)00199-8
44. P. Manjula, R. Boppella, and S. Manorama, ACS Appl. Mater. Interfaces **4**, 6252 (2012). http://dx.doi.org/10.1021/am301840s
45. C. Shifu and C. Gengyu, Solar Energy, **79**, 1 (2005). http://dx.doi.org/10.1016/j.solener.2004.10.006
46. S. Dai and Z. Yao, Appl. Surf. Sci. **258**, 5703 (2012). http://dx.doi.org/10.1016/j.apsusc.2012.02.065